JACS
JOURNAL OF THE AMERICAN CHEMICAL SOCIETY
pubs.acs.org/JACS

Article

Genetically Encoded Pentafluorophenylalanine Enables Quantitative Probing of Local Protein Malleability by ^{19}F NMR

Nathan Paul, Adarshi P. Welegedara, Rebecca L. Frkic, Luca Macri, Toby R. C. Thompson, James L. Baber, Edan Habel, Elwy H. Abdelkader, Haocheng Qianzhu, Nicholas F. Chilton, Colin J. Jackson, Ad Bax, Thomas Huber, and Gottfried Otting*

Cite This: J. Am. Chem. Soc. 2026, 148, 32644−32655

ABSTRACT: Aromatic ring flips in proteins provide a direct probe of local structural fluctuations, yet their rates are typically too fast for quantitative measurement by NMR spectroscopy. Here we show that site-specific incorporation of 2,3,4,5,6-pentafluoro-L-phenylalanine (F_5Phe) reshapes the torsional energy landscape of aromatic side chains, slowing ring flips by over 2 orders of magnitude and shifting them into the slow-exchange regime accessible by ^{19}F NMR. F_5Phe can be genetically encoded with high fidelity and minimal structural perturbation, as confirmed by high-resolution X-ray crystallography across multiple proteins. The resulting ^{19}F NMR spectra enable direct, quantitative measurements of ring-flip kinetics without the need for isotope labeling or complex multidimensional experiments. Application to a diverse set of proteins demonstrates that ring-flip rates vary widely even within the same hydrophobic cluster, revealing highly localized conformational fluctuations rather than global unfolding events. Pressure-dependent measurements yield small activation volumes, indicating that the structural rearrangements enabling ring flips are spatially confined. Ligand binding and protein−protein interactions modulate ring-flip rates in a site-specific manner, providing a sensitive readout of allosteric effects on local protein malleability. These results establish fluorinated aromatic amino acids as a general chemical strategy to engineer dynamic observables in proteins, transforming aromatic ring flips into a broadly applicable probe of local conformational dynamics and allostery.

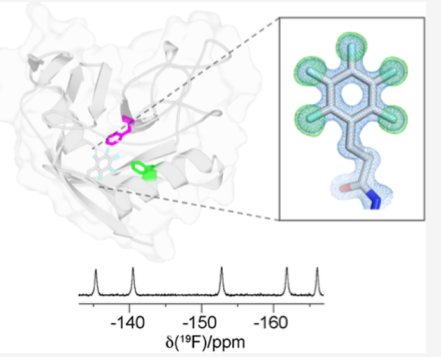

INTRODUCTION

Aromatic residues play central roles in protein−ligand recognition and catalysis due to their conformational rigidity and well-defined packing interactions.[1] They exhibit distinct dynamical regimes: solvent-exposed rings undergo near-continuous rotational diffusion,[2] whereas buried residues typically undergo discrete 180° flips about the C^{β}−C^{γ} bond.[3] Aromatic ring flips thus provide a unique probe of local structural malleability.

As the start and end states of a ring flip are structurally indistinguishable, nuclear magnetic resonance (NMR) spectroscopy is the only technique capable of measuring flip rates quantitatively. Classical ^{1}H NMR analyses classify ring flip dynamics into slow, intermediate, or fast exchange regimes depending on the relationship between flip rates and chemical shift differences.[4,5]

Quantitative measurements of aromatic ring flips have been reported for several proteins, but mostly for relatively small systems.[5−12] This limitation arises both from spectral overlap in larger proteins and the fact that aromatic ring flips are typically too fast to measure, even for deeply buried residues.[2,13] Although relaxation dispersion experiments can access fast exchange regimes for some of the more slowly flipping rings, they require more complex data acquisition and analysis.[10,14−16]

Aromatic ring flips are much easier to characterize in the slow exchange regime.[13] However, this regime is usually accessible only under special conditions, such as the presence of covalent cross-links or tightly binding ligands, high pressure,[3,7] low temperature,[17] or in the solid state.[18] An alternative approach is chemical modification. For example, 2,6-difluoro-L-tyrosine residues can slow ring flips sufficiently to enter the slow exchange regime under physiological conditions.[19] This effect has been attributed to steric interactions between fluorine atoms and the protein backbone.

Fluorination offers additional advantages, including straightforward detection by one-dimensional ^{19}F NMR spectroscopy and minimal structural perturbation due to the geometric similarity between C−F and C−H bonds. The van der Waals radius of fluorine (~1.47 Å) is only slightly larger than that of

Received: May 18, 2026
Revised: June 25, 2026
Accepted: June 30, 2026
Published: July 24, 2026

https://doi.org/10.1021/jacs.6c10121
J. Am. Chem. Soc. 2026, 148, 32644−32655

hydrogen, and carbon-bound fluorine is a weak hydrogen-bond acceptor,[20] allowing incorporation into hydrophobic protein cores. Nonetheless, multiple substitutions may unpredictably affect protein structure, stability, and dynamics, making site-specific incorporation desirable.

Genetic encoding systems now enable site-specific incorporation of fluorinated aromatic amino acids, including tyrosine and phenylalanine analogues.[21−30] Among these, 2,3,4,5,6-pentafluoro-L-phenylalanine (F_5Phe; Figure 1) offers excellent orthogonality relative to Phe and can be incorporated efficiently using engineered aminoacyl-tRNA synthetases.[25,28]

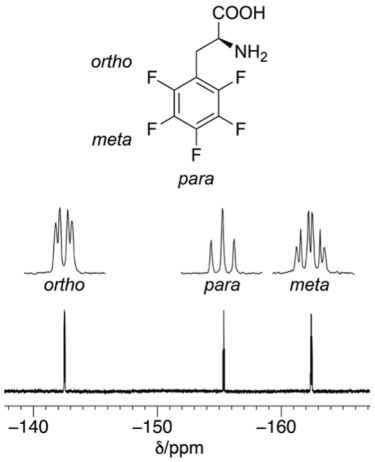

Figure 1. Chemical structure and ^{19}F NMR spectrum of 2,3,4,5,6-pentafluoro-L-phenylalanine (F_5Phe). The NMR spectrum was recorded at 25 °C in phosphate-buffered saline at pH 7.4 using a 400 MHz NMR spectrometer. Multiplet fine structures are shown in expanded views above the spectrum. The assignment (low-field to high-field) is *ortho*, *para*, and *meta*. The multiplets are broad due to large $^3J_{FF}$ and $^5J_{FF}$ couplings,[31] with the sum of the couplings adding to 30, 42, and 51 Hz, respectively.

Previous crystallography studies on the villin headpiece subdomain indicate that single Phe → F_5Phe substitutions are well tolerated with minimal perturbation of the overall fold and preserved local side-chain conformations.[32] Although the C_6F_5 group occupies a larger volume than a phenyl ring (141 Å^3 for C_6F_5H versus 106 Å^3 for C_6H_6), it can be accommodated within the hydrophobic core with only modest effects on stability.[33,34]

Here, we demonstrate that single Phe → F_5Phe substitutions enable quantitative measurements of aromatic ring flip rates in proteins by shifting the dynamics into the slow exchange regime accessible by ^{19}F NMR. We validate this approach across multiple proteins, assess structural perturbations by X-ray crystallography, compare genetic encoding systems, and show that F_5Phe residues can serve as minimally invasive probes of local protein malleability and allosteric effects.

RESULTS

Calculations Predict Slower Ring Flips in F_5Phe than Phe

The C_6F_5 group of the F_5Phe amino acid is expected to rotate more slowly than the phenyl ring of Phe due to greater steric hindrance. Modeling the side chain with fixed bond geometries, the ring rotation brings the *ortho* fluorine atoms as close as 1.6 Å of the H^α atom, within 2.3 Å of the H^β atoms, and within 2.2 Å of the C^α atom. These distances are shorter than the sum of the respective van der Waals radii. The ring rotation of Phe generates similarly short distances (within 0.1 Å), but the smaller van der Waals radius of hydrogen reduces the severity of the steric clashes. Different backbone conformations potentially create further steric clashes during the ring rotation (Figure S1).

A quantitative assessment of the energy potential of aromatic ring rotations is afforded by density functional theory (DFT) calculations of ethylbenzene and pentafluoroethylbenzene (Figure 2). Proximity of a fluorine atom to the methyl group

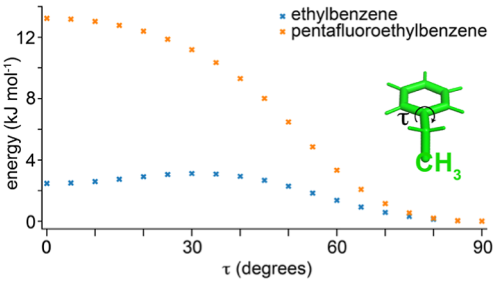

Figure 2. DFT calculations of the energy barrier for rotation of the phenyl ring in ethylbenzene (blue points) and the pentafluorophenyl ring in 1-ethyl-2,3,4,5,6-pentafluoroethylbenzene (orange points) relative to the energy for τ = 90°. The dihedral angle τ refers to the C−C−C−C fragment centered on the Ph−C bond in $PhCH_2CH_3$. It corresponds to the χ_2 angle in phenylalanine. The inset illustrates the conformation for τ = 90°.

(τ = 0°) presents a notably greater energy penalty than proximity to the hydrogen atoms of the CH_2 group (τ = 60°). Therefore, side chain conformations near χ_2 = 0°, which are already infrequent for Phe residues,[35] are further disfavored for F_5Phe residues. The difference in barrier heights, ΔE, implies that the flip rate of the C_6F_5 group at 25 °C intrinsically is about 60-fold slower than that of the phenyl ring based on proportionality to $\exp(-\Delta E/RT)$, where R is the gas constant and T the temperature.

Genetic Encoding of F_5Phe

Several systems have been established for the genetic encoding of F_5Phe in *Escherichia coli*.[24−27] To compare their relative performance in terms of protein yield and orthogonality with regard to canonical amino acids, we used red fluorescent protein (RFP) preceded by the T7 bacteriophage gene 10 expression tag,[36] a His_6 tag, and the site for the noncanonical amino acid defined by an amber stop codon (Table S1). The best performing systems were the pyrrolysyl-tRNA synthetase mutants derived from *Methanosarcina barkeri* (*Mb*)[26] and the methanogenic archaeon ISO4-G1,[29] for which intact protein mass spectrometry confirmed excellent orthogonality with respect to canonical amino acids (Figure S2). In the present work, we used the ISO4-G1 variant 09 to generate all F_5Phe mutants. Although protein yields varied (Table S2), full orthogonality was maintained (Figure S3).

Stability of Proteins Containing a Single F_5Phe Residue

The present work explored the ring flip rates of F_5Phe residues in seven different proteins, in total probing 14 different phenylalanine sites (Table S1), including protein−ligand complexes for six systems. For single-domain proteins, we determined melting temperatures to probe the effect of the Phe → F_5Phe substitution on protein stability. Table 1 shows that

https://doi.org/10.1021/jacs.6c10121
J. Am. Chem. Soc. 2026, 148, 32644−32655

the presence of an F_5Phe residue can be either destabilizing or stabilizing, consistent with previous observations.[32]

Table 1. Melting Temperatures T_m of Wild-Type Proteins and F_5Phe Mutants

protein	site of F_5Phe (residue number)	T_m (°C)
PpiB	wild-type	51[a]–52[b,c]
	F4	46[a]
	F27	43[a]
	F98	47[a]
GB1	wild-type	81[b,d]
	F30	53[b]
	F52	63[b]
Arc-NL	wild-type	67[b]
	F267	67[b]
	F271	73[b]

[a]Determined by differential scanning fluorescence (DSF; Figure S4). [b]Determined by CD spectroscopy (Figure S5). [c]From Tan et al. (2024).[37] [d]From Tan et al. (2025).[38]

Structural Conservation of the Conformations of F_5Phe Residues

To assess structural perturbations caused by F_5Phe, crystal structures were determined for two proteins. In *E. coli* peptidyl–prolyl *cis–trans* isomerase B (PpiB), substitution of residue F4 by F_5Phe preserves the local structure (Figures 3a and S6a) with only minor changes in the χ_1 and χ_2 angles (<14°). Despite the predicted energy penalty for this conformation (χ_2 = −28°; Figure 2), the structure is essentially conserved, demonstrating that the C_6F_5 group is well accommodated despite the predicted energy penalty of ∼8 kJ/mol relative to χ_2 = 90°.

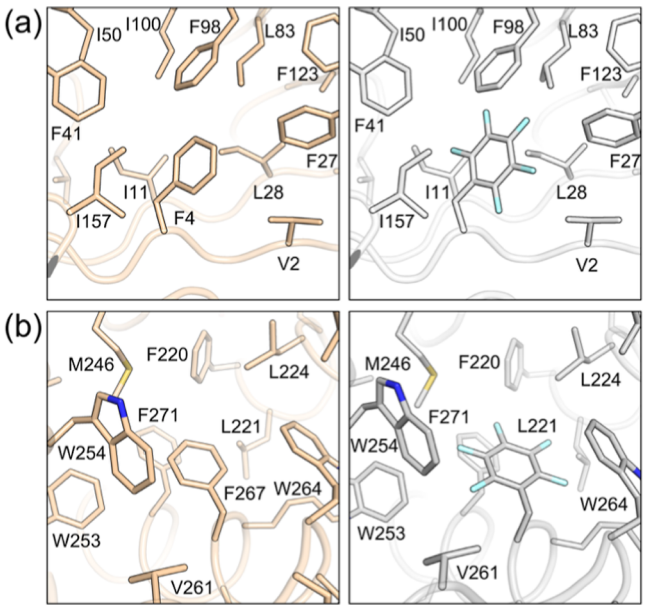

Figure 3. Comparisons of single crystal structures of wild-type proteins (wheat) and F_5Phe mutants (gray) illustrating the structural conservation in the vicinity of the F_5Phe residue. The C–F bonds of the F_5Phe residues are colored cyan. (a) Site of F4 in PpiB (PDB IDs 2NUL[39] and 26AO). (b) Site of F267 in Arc-NL in complex with the nanobody H11 (PDB IDs 8QF4[40] and 26AP).

Similarly, in the cocrystal of the N-lobe of Arc (Arc-NL) with the nanobody H11, substitution of F267 by F_5Phe preserves both side-chain conformation (χ_1 and χ_2 changes <4°) and local environment (Figures 3b and S6b). These results show that single F_5Phe substitutions cause minimal structural perturbation.

^{19}F NMR Spectroscopy of F_5Phe Residues in Proteins

The ^{19}F NMR spectrum of the free F_5Phe amino acid (Figure 1) spans 20 ppm and shows fast ring rotation, resulting in averaged *ortho* and *meta* fluorine signals. Five ^{19}F resonances are expected in the slow exchange regime, with exchange broadening affecting the *ortho* and *meta* signals but not the *para* fluorine. T_1(^{19}F) relaxation times in proteins were about 300 ms. To maximize sensitivity, we typically used recovery delays of 0.5 s.

F_5Phe in PpiB

PpiB is a 19 kDa protein containing 12 Phe residues, making their resonance assignment challenging without isotope labeling. To probe aromatic ring flips in a buried hydrophobic cluster, F4, F27, and F98 in PpiB were individually replaced by F_5Phe (Figure 4a). The ^{19}F NMR spectra show chemical shift dispersion of up to 30 ppm (Figure 4b).

F_5Phe in position 4 displays three signals, indicating fast ring flips. In contrast, positions 27 and 98 show five signals, consistent with slow exchange. Position 27 also exhibits peak shoulders, indicating conformational heterogeneity.

[^{19}F,^{19}F]-NOESY spectra confirm assignments, with the central resonance corresponding to the *para* fluorine (Figure 4c). No exchange cross-peaks are observed for position 27, indicating very slow flipping (<0.1 s^{-1}), whereas position 98 shows cross-peaks corresponding to ∼150 s^{-1}.

To compare with the wild-type protein, 4F-Phe was introduced at the same sites. ^{1}H–^{19}F correlation spectra reveal single resonances for the $^1H^{\varepsilon}$ spins (Figure S7), consistent with fast ring flips. A narrower line width for position 4 indicates the fastest rotation, in agreement with the F_5Phe results.

F_5Phe in GB1

To probe a protein with known flip rates of canonical Phe residues, we investigated F_5Phe in the protein G B1 domain (GB1). F30 and F52 form part of the hydrophobic core with little access to solvent (Figure 5a). [^{1}H,^{1}H]-NOESY spectra of the F_5Phe mutants confirmed conservation of the protein fold. The 1D ^{19}F NMR spectra show five resonances characteristic of the slow exchange regime. The *para* fluorines show much narrower signals than the *ortho* and *meta* fluorines, confirming exchange broadening by ring flips rather than other phenomena. [^{19}F,^{19}F]-NOESY spectra, recorded with mixing times sufficiently short that the exchange cross-peaks were significantly weaker than the diagonal peaks, indicate flip rates of 60 and 800 s^{-1} in positions 30 and 52, respectively (Figure 5). At the same temperature (25 °C), much faster flipping has been reported for the wild-type protein, i.e., 20,000–40,000 s^{-1} for F30 and 20,000–70,000 s^{-1} for F52.[12,42]

F_5Phe in the Arc-NL/H11 Complex

To measure changes in ^{19}F chemical shifts and flip rates in a protein–protein complex, we investigated F_5Phe in the Arc-NL/H11 complex. Biolayer interferometry (BLI) experiments confirmed that H11 retained full affinity to the Arc-NL F_5Phe mutants in positions 267 and 271 (Figure S8, Table S5). F267 is buried in the hydrophobic core of Arc-NL, whereas F271 is located at the protein–protein interface (Figure 6e). The ^{19}F

https://doi.org/10.1021/jacs.6c10121
J. Am. Chem. Soc. 2026, 148, 32644–32655

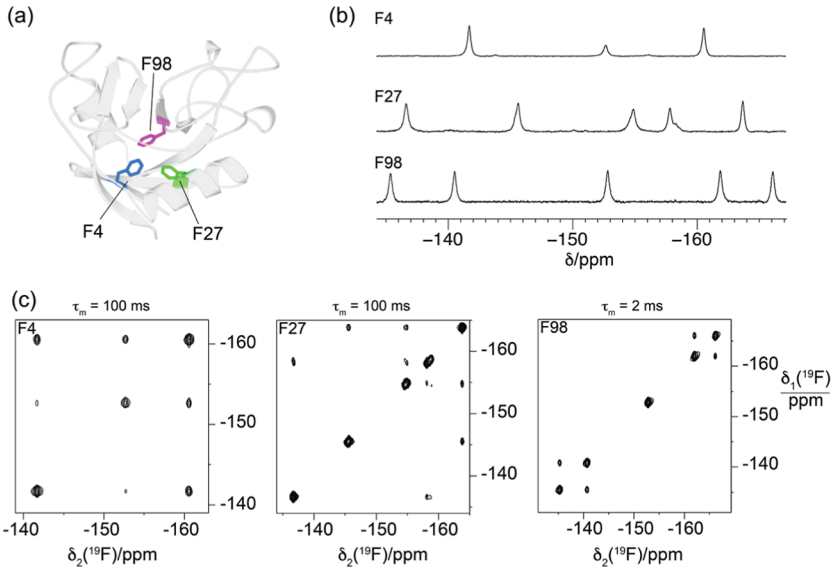

Figure 4. ^{19}F NMR spectra of PpiB with F_5Phe replacing F4, F27, or F98. (a) Structure showing the sites of the F_5Phe mutations. (b) 1D ^{19}F NMR spectra recorded at 25 °C on a 600 MHz NMR spectrometer and processed with 10 Hz line broadening (c) [^{19}F,^{19}F]-NOESY spectra recorded on a 400 MHz NMR spectrometer. The spectra are annotated with the mixing time used and the site of F_5Phe incorporation. Acquisition parameters are provided in Table S4.

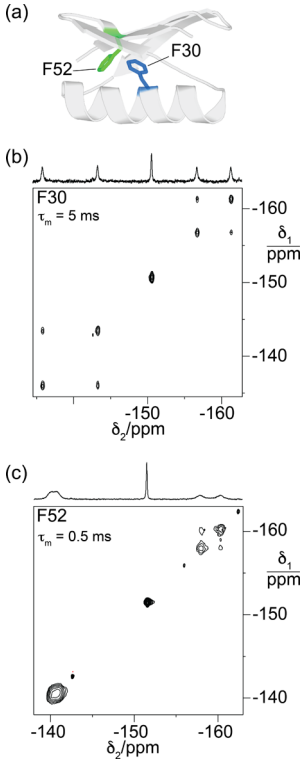

Figure 5. Ring flips of F_5Phe in positions 30 or 52 of GB1 are in the slow exchange regime at 25 °C. (a) Structure of GB1 (PDB ID 2QMT)[41] showing the sites of the F_5Phe mutations. (b) [^{19}F,^{19}F]-NOESY spectrum of F_5Phe in position 30. The mixing time is indicated in the spectrum and the 1D ^{19}F NMR spectrum is shown above. (c) Same as (b) but for position 52. Narrow signals at −142.6, −156.0, and −162.5 ppm correspond to traces of denatured protein.

NMR spectrum of the F267/F_5Phe mutant indicates ring flips in the slow exchange regime, which slow further in the complex with H11 (Figure 6a). In the free protein, the difference in line widths of the *ortho* and *meta* fluorines compared with the *para* fluorine (~550 Hz) indicates a flip rate of ~1700 s^{-1}, which slows about 100-fold in the complex with H11 (16 s^{-1}; Figure 6d). This suggests rigidification of the Arc-NL structure in the complex.

In contrast, H11 affects the ring flip in position 271 much less (Figure 6b), showing that the nanobody−antigen interface retains motional flexibility. In the complex, the difference in line widths (~200 Hz) indicates a ring flip rate of ~600 s^{-1}.

F_5Phe in position 70 of H11 is in the fast exchange regime both in the free protein and the complex with Arc-NL. All three ^{19}F resonances respond to the binding of Arc-NL with significant chemical shift changes, despite F70 being more than 10 Å from the nearest atom of Arc-NL. The F_5Phe residue hidden in the core of H11 thus acts as an allosteric sensor of the remote antigen−nanobody interaction.

F_5Phe in FKBP-12, Maltose Binding Protein, and a Flaviviral Protease

To further assess the potential of allosteric sensing by buried F_5Phe residues, we incorporated F_5Phe residues in the FK506 binding protein 12 (FKBP-12; ligand rapamycin), *E. coli* maltose binding protein (MBP; ligand maltose), and the dengue virus (serotype 2) NS2B−NS3 protease (DENV; ligand aprotinin). In wild-type FKBP-12, all Phe and Tyr residues are in the fast exchange regime[10] and exchange broadenings observed for F48 and F99 have been attributed to a tautomer equilibrium of H87 rather than ring flipping.[15] In the complex with rapamycin, ^{1}H NMR at 10 °C observed F48 in the intermediate and F99 in the slow exchange regime (flip rate ~ 16 s^{-1}).[10] The F_5Phe mutants showed much slower flip rates, with slow exchange in position 48 already in the free protein (flip rate ~ 11 s^{-1}) and even slower exchange in the complex with rapamycin (Figures 7a and S9a). Position 99 is in the fast exchange limit in the free protein (Figure 7a) while the complex with rapamycin showed no exchange cross-peaks in the [^{19}F,^{19}F]-NOESY spectrum (flip rate < 3 s^{-1}). These results confirm that rapamycin greatly rigidifies the structure of FKBP-12.[10]

https://doi.org/10.1021/jacs.6c10121
J. Am. Chem. Soc. 2026, 148, 32644−32655

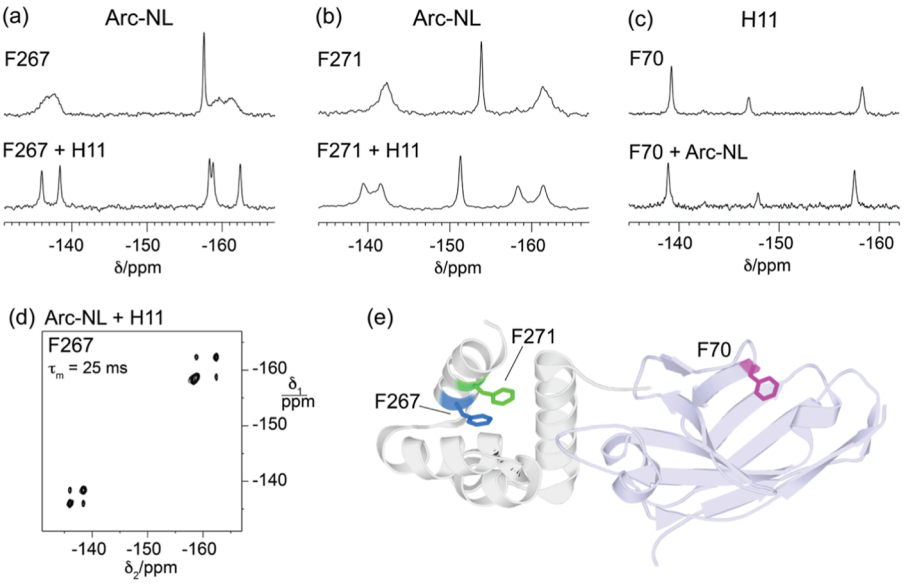

Figure 6. Nanobody–antigen interactions alter the ^{19}F chemical shifts and ring flip rates of F_5Phe residues. (a) 1D ^{19}F NMR spectra of free Arc-NL F267/F_5Phe and the 1:1 complex with H11. Spectra recorded at 25 °C on a 400 MHz NMR spectrometer. Upper panel: free protein. Spectrum processed with 50 Hz line broadening. Lower panel: 1:1 complex with H11. Spectrum processed with 70 Hz line broadening. (b) Same as (a), but for the Arc-NL F271/F_5Phe mutant. (c) Same as (a), but for the H11 F70/F_5Phe mutant and Arc-NL added in small excess. Spectra processed with 30 Hz line broadening. (d) [^{19}F,^{19}F]-NOESY spectrum of the Arc-NL F267/F_5Phe mutant in complex with H11. The mixing time is indicated in the spectrum. (e) Cartoon representation of the Arc-NL/H11 complex (PDB ID 8QF4).[40]

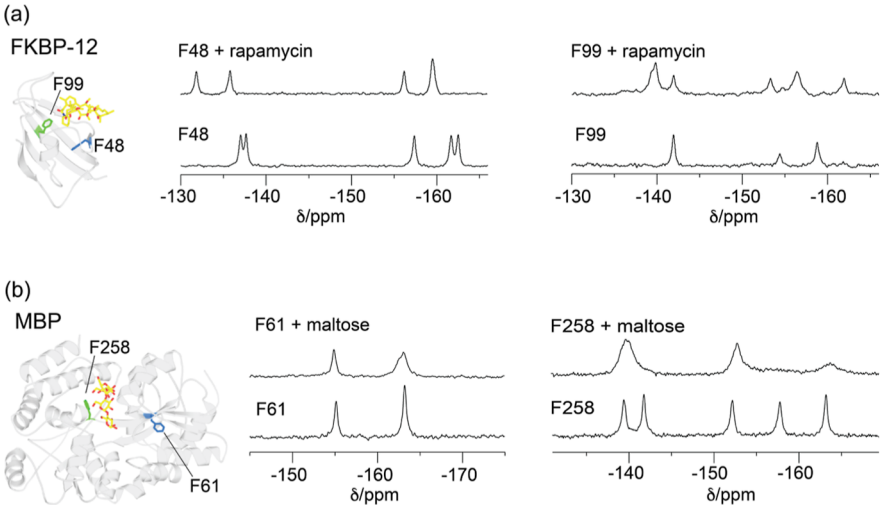

Figure 7. 1D ^{19}F NMR spectra of F_5Phe mutants of FKBP-12 and MBP. (a) FKBP-12 with F_5Phe in positions 48 or 99. The spectra were recorded on a 400 MHz NMR spectrometer and processed with 50 Hz line broadening. Due to precipitation at 25 °C, the samples were measured at 10 °C. Lower panel: free protein. Upper panel: spectrum of the complex with rapamycin. The cartoon (PDB ID 1FKB)[43] shows the locations of F48 and F99 in blue and green, and rapamycin in yellow and red. (b) MBP with F_5Phe in positions 61 or 258, with and without a 2-fold excess of maltose measured at 25 °C. The F61/F_5Phe mutant was recorded on a 400 MHz NMR spectrometer. Processed with 50 Hz line broadening. The F258/F_5Phe mutant were recorded on a 500 MHz NMR spectrometer with a cryoprobe. Processed with 40 Hz line broadening. The cartoon drawing (4MBP)[44] shows the locations of the mutation sites, and maltose in yellow and red.

^{19}F NMR of selectively ^{19}F labeled proteins readily detects minor conformational species as indicated by the additional small peaks observed by position 99 in the FKBP-12/rapamycin complex (Figure 7a). Another example for additional small peaks is the F116/F_5Phe mutant of the NS2B–NS3 protease from the dengue virus serotype 2 (DENV; Figure S10). Minor species are common in flaviviral NS2B–NS3 proteases and attributed to slow flips of tryptophan side chains.[28,29] F_5Phe produces more homogeneous spectra than singly or doubly fluorinated Phe residues installed at the site of F116,[29] suggesting lesser structural perturbation by F_5Phe.

MBP has a molecular weight of 40.7 kDa and the assignments of the aromatic side chains are incomplete. Available information for F61 and F258 indicates ring flips in the fast exchange limit.[45] F_5Phe in position 61 displays fast exchange and position 258 a slow flip rate of 45 s^{-1} (Figures 7b and S9b). Crystal structures of MBP with and without maltose show high structural conservation for F61 and its environment.[44,46] Nonetheless, maltose changes the chemical shifts in position 61 despite the fluorine atoms being over 8 Å from the nearest maltose atom. For F258, the crystal structures show significant changes in the environment induced by maltose and

https://doi.org/10.1021/jacs.6c10121
J. Am. Chem. Soc. 2026, 148, 32644–32655

the ^{19}F NMR spectrum of the F258/F_5Phe mutant collapses into three main signals, suggesting accelerated ring flips (Figure 7b). A [^{19}F,^{19}F]-NOESY spectrum of the complex (Figure S9b) shares its cross-peak pattern with the corresponding spectrum of the PpiB F4/F_5Phe mutant (Figure 4c), suggesting that the *meta* signal is unexpectedly weak, which may be explained by the broad peak at −157 ppm (Figure 7b) representing a second environment. The peak widths signal a heterogeneous environment exchanging in the slow to intermediate time regime.

Criteria for Ring Flips in the Slow Exchange Regime

To predict whether an F_5Phe residue flips in the slow motional regime, we modeled the Phe → F_5Phe substitution by replacing the corresponding C−H bonds in the protein structure by C−F bonds and visualized severe steric clashes using the program PyMOL. The cutoffs used were sufficiently stringent to exclude the intraresidual F−C$^{\alpha}$ distance associated with $\chi_2 = 0°$ as a clash (2.46 Å; Figure 2). By these criteria, the starting conformations accommodated the fluorine atoms, but ring rotation led to steric clashes (Figure 8). No consistent correlation was observed between the magnitude of the van der Waals violations and the ring flip rate, irrespective of whether hydrogen coordinates were included.

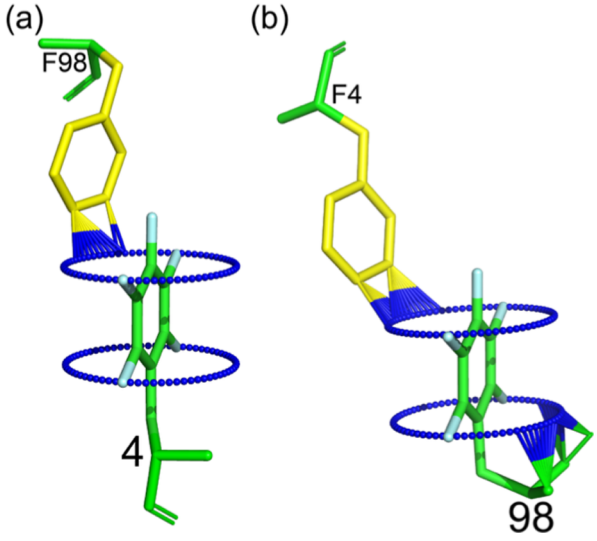

Figure 8. Ring rotation model of the PpiB mutants F4/F_5Phe and F98/F_5Phe based on the crystal structure 2NUL.[39] Color code: backbone atoms and F_5Phe residue in green (fluorine in cyan), Phe side chain in yellow. The positions of the *ortho* and *meta* fluorine atoms during rotation about the C$^{\beta}$−C$^{\gamma}$ bond (changing χ_2 in steps of 5°) are marked by blue spheres. The figure was produced with the program PyMOL,[47] which highlights severe steric clashes of the fluorine positions (distances d_{FO} < 2.00 Å, d_{FN} < 2.05 Å, d_{FC} < 2.10 Å, d_{FS} < 2.35 Å) by drawing unphysical bonds.

The number of predicted steric clashes proved a useful indicator for slow ring flips as exemplified by the three F_5Phe mutants of PpiB (Table 2). In the case of FKBP-12, however, seven clashing atoms are not sufficient to bring the F99/F_5Phe mutant into the slow exchange regime, which can be explained by the solvent accessible surface area (SASA) of the phenyl ring at this site as solvent-exposed side chains are in a structurally more flexible environment. Other examples of partially solvent exposed side chains are F30 and F52 in GB1 (slow ring flip), F116 in the DENV NS2B−NS3 protease (fast ring flip), and F258 in free MBP (slow ring flip). Among these, the fewest clashing atoms are predicted for the DENV protease, which shows fast ring flips.

Intraresidual clashes with backbone atoms seem to exert a particularly efficient brake on ring rotations. Indeed, all slow ring flips observed in the present work are hindered by intraresidue clashes with backbone atoms (highlighted in bold in Table 2). The only exceptions are the slow ring flips in position 30 of GB1 and in position 258 of MBP. In both cases, the ring rotation causes clashes with many atoms. In the apo structure of MBP, F258 is hemmed in between two rigid tryptophan side chains (Figure S11).

Altering Activation Volumes by Complex Formation

According to Eyring transition state theory, the increase in volume of the transition state, $\Delta V^{\ddagger}$, can be determined from measurements of the aromatic ring flip rates k as a function of pressure p using the relationship

$$\delta \ln k/\delta p = -\Delta V^{\ddagger}/k_B T \quad (1)$$

where k_B is the Boltzmann constant and T the temperature.[3] Figure 9a,b shows pressure-dependent NMR spectra of the Arc-NL F267/F_5Phe mutant recorded in the absence and presence of the nanobody H11. The measurements were performed at 5 °C to improve the spectral resolution and guard against unfolding. The ring flip rate decreased with increasing pressure, most pronounced at higher pressures (Figure 9c). A linear fit to all data points yields an activation volume of 29 ± 4 Å^3, but only 12 ± 13 Å^3 if the pressure range is limited to 1 kbar and below. These volumes are notably smaller than the volume swept by the rotating aromatic ring, which is about twice as large as the volume of the C_6F_5 group itself.

In the complex with the nanobody H11, Arc-NL is more stable toward unfolding and position 267 displays five resolved peaks at 25 °C. The pressure dependent ring flip rates correspond to an increased activation volume of 68 ± 3 Å^3 (Figure 9c). This indicates that the nanobody blocks the usual reaction path for the ring flip in the free protein in favor of a path characterized by a larger activation volume.

Interestingly, the ^{19}F chemical shifts changed greatly with hydrostatic pressure (Figure 9a,b). For comparison, the ^{1}H chemical shift of water changes by less than 0.03 ppm between 1 and 2000 bar.[51] The similar magnitude in chemical shift changes observed for free and H11-bound Arc-NL indicates that the equilibrium structure of Arc-NL responds to pressure in the same way in both states.

DISCUSSION

Probing Ring Flip Rates Using F_5Phe

The BioMagResBank reports degenerate chemical shifts for the vast majority of Phe and Tyr rings, indicating rapid ring flips at ambient temperature.[17] Even in the case of aprotinin (BPTI), which is a protein stabilized by multiple disulfide bonds, ring flip rates could be determined quantitatively for only 3 of 8 aromatic residues,[52] a finding that also holds at subzero temperatures.[17]

Fluorination slows ring flip rates, greatly facilitating their measurement as reported previously by Li and co-workers for Tyr residues.[19] F_5Phe has multiple advantages for probing aromatic ring flips. (i) Phenylalanine is less hydrophilic than tyrosine and therefore more easily buried in the hydrophobic core, where the impact of an F_5Phe residue on the surface

https://doi.org/10.1021/jacs.6c10121
J. Am. Chem. Soc. 2026, 148, 32644−32655

Table 2. Steric Clashes Predicted in Models of Ring Rotation of F_5Phe Residues and Experimentally Observed Ring Flip Rates[a]

protein, PDB ID, and residue	atoms contacting F[δb]	atoms contacting F[ε]	total number of clashing atoms[b]	SASA (Å^2)[c]	χ_2 (degrees)	experimental ring flip rate
PpiB (2NUL)						
F4	none	$F_{98}C^{\varepsilon1}/C^{\zeta}$	2	0	−24	fast
F27	**$F_{27}C'/O$**, $F_{123}C^{\delta2}/C^{\varepsilon2}/C^{\zeta}$	$C_{31}S^{\gamma}$	6	0	64	very slow (<0.1 s^{-1})
F98	**$F_{98}N/C'/O$**	$F_4C^{\varepsilon2}/C^{\zeta}$	5	0	83	slow (150 s^{-1})
GB1 (2QMT)						
F30	$L_5C^{\beta}/C^{\gamma}/C^{\delta2}$, $A_{26}O$	K_4C', L_5N/C^{β}, $T_{18}C^{\beta}/C^{\gamma2}$	8	6	−35	slow (60 s^{-1})
F52	$F_{30}C^{\delta2}/C^{\varepsilon2}$, $Y_{45}C^{\delta1}$, **$F_{52}N$**	$E_{27}N/C^{\alpha}/C^{\beta}$, $Y_{45}C^{\gamma}/C^{\delta1}/C^{\varepsilon1}$	9	9	80	slow (800 s^{-1})
Arc-NL/H11 (8QF4)						
F267 (Arc-NL)	$I_{242}C^{\delta1}$, **$F_{267}C'/O$**, $K_{268}N$	$I_{242}C^{\gamma2}$, $F_{271}C^{\beta}$	6	0	72	intermediate (1700 s^{-1}), slow in complex (16 s^{-1})
F271 (Arc-NL)	$L_{221}C^{\delta2}$, $F_{267}C^{\zeta}$, **$F_{271}C'/O$**	$F_{220}C^{\delta2}/C^{\varepsilon2}$, $S_{275}C^{\beta}/O^{\gamma}$	8	0	74	intermediate, little slower in complex (600 s^{-1})
F70 (H11)	$V_{66}C^{\beta}/C^{\gamma1}$, $M_{85}C^{\alpha}$,C^{γ}	$M_{85}C^{\beta}/C^{\gamma}/S^{\delta}$	4	0	16	fast
FKBP-12/rapamycin (1FKB)						
F48[d]	$F_{46}C^{\varepsilon2}$, **$F_{48}N/C'/O$**, $M_{49}N$, $V_{55}C^{\gamma1}$	$C_{22}C^{\beta}/S^{\gamma}$, $W_{59}C^{\varepsilon3}$	9	0	−79	slow (11 s^{-1}), very slow with rapamycin (<1 s^{-1})
F99[d]	$G_{28}C^{\alpha}$, $W_{59}N^{\varepsilon1}/C^{\varepsilon2}/C^{\zeta2}$, $V_{98}C'/O$	$F_{36}C^{\zeta}$	7	11	87	fast, very slow with rapamycin (<3 s^{-1})
MBP (1OMP)						
F61	$I_{11}C^{\delta1}$, $I_{60}C'$	$L_{20}C^{\delta2}$, $I_{59}C^{\delta1}$, $A_{264}C^{\beta}$	5	5	84	fast
F258	$M_{330}C^{\gamma}$	$W_{158}C^{\gamma}/C^{\delta1}/N^{\varepsilon1}/C^{\varepsilon2}$, $M_{336}C^{\varepsilon}$, $W_{340}C^{\eta2}$	7	0.1	−60	slow (45 s^{-1})
MBP/maltose (4MBP)						
F61	$I_{11}C^{\delta1}$, $S_{263}O$	$A_{264}C^{\beta}$	3	6	86	fast
F258	$W_{158}C^{\delta1}/N^{\varepsilon1}$, $M_{330}C^{\gamma}$	$W_{158}N^{\varepsilon1}/C^{\varepsilon2}/C^{\zeta2}$, $P_{331}C^{\delta}$	7	1	−38	fast, broad lines indicating complex dynamics
DENV protease (2FOM)[e]						
F116	**$F_{116}N$**, $L_{115}C/O$, $T_{156}C^{\gamma2}$	$V_{162}C^{\gamma2}$	5	62	83	fast
WNV protease/aprotinin (2IJO)[e]						
F116	$V_{77(NS2B)}C^{\gamma2}$, $A_{125}C^{\beta}$	$I_{162}C^{\gamma2}$, $A_{164}N$	4	0.4	14	n/a

[a]Indicating the Phe residue substituted by F_5Phe. Steric clashes were predicted by changing the χ_2 angle of the F_5Phe residue in steps of 5° and using PyMOL to report unduly short interatomic distances as bonds, considering heavy atoms only (Figures 8 and S11). Intraresidual clashes of the C_6F_5 ring with backbone atoms are highlighted in bold. The experimental ring flip rate is reported as fast, intermediate or slow depending on the appearance of the ^{19}F NMR spectrum, showing either three lines, strongly broadened lines, or five resolved lines, respectively. [b]Excluding intraresidual contacts with C^{α}. [c]Solvent accessible surface area of the phenyl ring in the crystal structure. [d]Measured at 10 °C. [e]The structure 2FOM[48] shows the NS2B−NS3 protease in an inactive open conformation. The active closed conformation is represented by the homologous protein from the West Nile virus.[49,50]

structure and activity of the protein is minimal. The fluorination of Phe changes no side chain pK_a values whereas fluorination promotes ionization of the OH group of tyrosines. (ii) F_5Phe combines increased space requirement and moment of inertia to create slow flip rates. The energy barrier imposed by the intraresidual $C^{\alpha}H$ and $C^{\beta}H_2$ groups significantly hinders the rotation. (iii) Measuring ring flip rates in the slow exchange regime is straightforward as exchange cross-peaks and diagonal peaks are readily resolved in a single 2D NOESY experiment. In contrast, [^{1}H,^{1}H]-NOESY spectra rarely display resolved diagonal peaks. Furthermore, comparison with the signal of the *para* fluorine, which is unaffected by ring flips, allows attributing the line broadenings of the *ortho* and *meta* fluorines to ring flips rather than alternative exchange phenomena. (iv) Altered ring flip rates demonstrate allosteric effects associated with ligand binding. (v) Efficient genetic encoding systems deliver F_5Phe mutants site-selectively and in high purity, rendering additional experiments for resonance assignment unnecessary. This is important for large proteins. (vi) The incorporation of single versus multiple F_5Phe residues minimizes the potential for structural and functional perturbations of the target protein. (vii) The chemical shift dispersion of the ^{19}F NMR signals of F_5Phe residues is large. The resulting spectral resolution enables measurements in large proteins without expensive isotope labeling. (viii) Due to their different properties, including size, electrostatic polarity, hydrophobicity, and polarizability, the ring-flip rates of C_6F_5 groups and corresponding phenyl rings in the wild-type protein do not correlate quantitatively, as illustrated by the data obtained for GB1. Nonetheless, in all examples of the present work, ring flips reported to be slow in the wild-type protein were also slow for the corresponding F_5Phe residues.

https://doi.org/10.1021/jacs.6c10121
J. Am. Chem. Soc. 2026, 148, 32644−32655

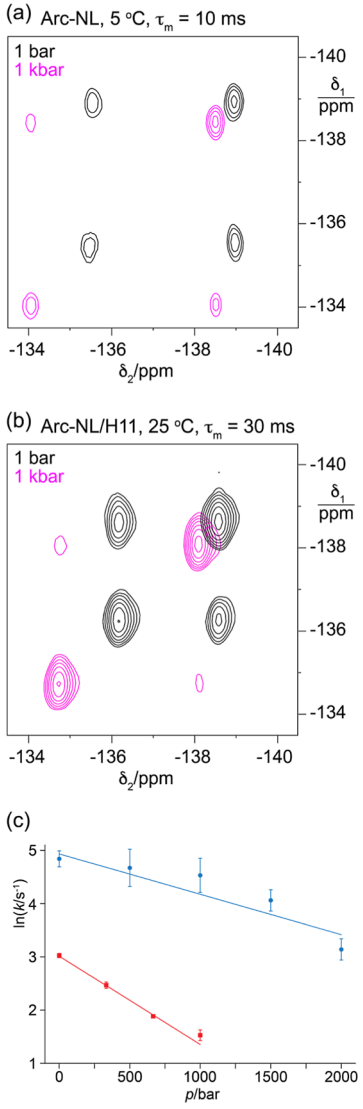

Figure 9. Hydrostatic pressure attenuates the ring flip in the Arc-NL F267/F_5Phe mutant more strongly in the complex with H11 than in the free protein. (a) [^{19}F,^{19}F]-NOESY spectrum of free Arc-NL at 5 °C. The spectral region shown contains the diagonal and exchange cross-peaks of the *ortho* ^{19}F resonances plotted with a factor of $\sqrt{2}$ between subsequent contour levels. The black and magenta spectra were recorded at atmospheric pressure and 1000 bar, respectively. (b) Same as (a) but for Arc-NL in complex with H11 at 25 °C. (c) Logarithmic plot of the flip rate, k (in s^{-1}), of F_5Phe in position 267 of Arc-NL in the free protein at 5 °C (blue points) and in the complex with H11 at 25 °C (red points). The linear fits shown correspond to activation volumes of 29 ± 4 Å^3 and 68 ± 3 Å^3, respectively. In the complex, measuring the very slow exchange rates at pressures ≥2000 bar or lower temperature (5 °C) was compromised by competition by ^{19}F−^{19}F NOEs. For the free protein, irreversible unfolding at high pressure required recording at 5 °C, while ring flip rates remained sufficiently fast for precise measurement.

Effects of F_5Phe on Protein Structure and Stability

F_5Phe residues are compatible both with hydrophobic and hydrophilic environments. F_5Phe is commonly considered as more hydrophobic than Phe,[53] although a revised hydrophobicity scale put F_5Phe in the vicinity of tyrosine.[54] In practice, Phe → F_5Phe substitutions are tolerated both in hydrophobic and solvent-exposed environments. The C_6F_5 ring lacks prominent electrostatic dipole moments that could destabilize a protein.

The effect of F_5Phe on the folding energies of small proteins and peptides has previously been found to be small (<4 kJ/mol) and both destabilizing and stabilizing.[33,55−57] The energy differences are similar in size as those reported for uniform substitutions of canonical aromatic residues by singly fluorinated analogues.[58,59] Similarly, the present work observed cases of destabilization and stabilization (Table 1).

Protein crystal structures show that aromatic amino acid side chains favor χ_2 angles near 90° (corresponding to τ = 90° in Figure 2).[35] Based on the DFT calculations of Figure 2, this bias should be slightly stronger for C_6F_5 rings. Nonetheless, the crystal structure of the PpiB F4/F_5Phe mutant confirms that χ_2 angles different from 90° are well tolerated, resulting in negligible structural impact of the F_5Phe residue on the protein structure (Figure 3a). In all examples of the present work, the proteins retained their capacity to bind ligands and other proteins.

GB1, FKBP-12, and Arc-NL showed evidence of slow irreversible protein unfolding but longevity was improved at lower temperatures. The remarkable capacity of bacterial protein synthesis to produce correctly folded proteins in vivo despite destabilizing mutations has been attributed to cotranslational folding on the ribosome favoring the fold of the wild-type protein.[60]

Ring Flip Rates as a Measure of Protein Malleability

Aided by large differences in ^{19}F chemical shifts, the intrinsically slower ring flips of fully buried F_5Phe residues often display ^{19}F NMR spectra in the slow exchange regime, which greatly facilitates the quantitative measurement of the flip rates. Combining solvent exposure and the number of expected clashes during ring rotation, especially with intra-residual backbone atoms, the chances of observing ring flips in the slow time regime can be predicted from crystal structures of the wild-type proteins. ^{19}F NMR measurements in the slow time regime cover flip rates differing by up to 3 orders of magnitude.

As shown by PpiB, different rings of the same hydrophobic cluster can flip with very different rates. This shows that the minimal protein dynamics opening the space required for the ring flip are bespoke for individual residues and thus highly localized events. If the ring flips were governed by an unfolding event that impacts an entire protein subdomain, different sites would be expected to appear more similar. Fast ring flips occurring despite clashes predicted with multiple other atoms thus indicate high local protein malleability. In contrast, immobilized aromatic rings indicate structural rigidity and by themselves constitute a rigid structural element.

Gaining an atomic resolution picture of the structural changes required for the flip of buried aromatic rings is challenging because the time scales involved exceed conventional molecular dynamics simulations. Recent metadynamics calculations applied to the small and disulfide-rich protein aprotinin suggested that aromatic ring flips are aided by changes in χ_1.[61] Evidence for this could be expected to be found in increased activation volumes.

Activation volumes of aromatic ring flips can be derived from the pressure dependence of flip rates. Published activation volumes of canonical aromatic residues range from 44 to 84 Å^3.[3,7,12,62] Based on the larger volume of C_6F_5 groups, correspondingly larger activation volumes would be expected

https://doi.org/10.1021/jacs.6c10121
J. Am. Chem. Soc. 2026, 148, 32644−32655

for F_5Phe residues. The experimentally determined activation volumes of F_5Phe in position 267 of Arc-NL, however, were small: 29 Å^3 in the free protein and 68 Å^3 in the complex with the nanobody. We speculate that the larger activation volumes reported previously for canonical amino acids arise from unusually stringent structural restraints required to establish the slow exchange regime. Interestingly, the activation volume of F_5Phe in position 267 of Arc-NL increases in the complex with the nanobody H11, showing that protein rigidification changes the dynamics required to open the void for the ring flip.

Aromatic ring flip rates are commonly interpreted by Eyring's transition state theory, which assumes an energy potential culminating in a single transition state. If multiple amino acid side chains need to give way for a ring flip to proceed, however, a more adequate description would involve multiple successive energy barriers and multiple pathways. This view is the basis of Kramers' theory,[63] which uses viscosity and a set of different activation enthalpies to describe diffusive processes associated with internal high-friction events in proteins.[64] Without the time resolution required to detect intermediates in the aromatic ring flip pathways, the Eyring transition state theory offers a simplifying interpretation. As the activation volumes obtained are system parameters, small activation volumes can arise from a mere redistribution of preexisting small void volumes in the protein.[65]

Allosteric Effects Detected by F_5Phe

When flip rates and ^{19}F chemical shifts of buried aromatic rings change in response to ligand binding at a remote site, this constitutes signaling in an allosteric manner. Interestingly, the nanobody H11 affected the flip rate in position 267 of Arc-NL much more than in position 271, despite the latter being closer to the interface (Figure 6e). In contrast, the chemical shift changes were more pronounced in position 271 (Figure 6a,b). This demonstrates that local malleability is a parameter complementary to the average structure governing the chemical shifts.

As globular proteins bind other proteins and ligands via surface residues, it is ideal if sensors can be installed in the core of the protein to leave the protein surface unaltered. For example, it has been shown that proteins can be endowed with visible fluorescence by substituting a tryptophan residue in the protein core by a 4-cyanotryptophan residue.[66] Depending on the protein structure, however, the cyano group can introduce significant steric clashes. Fluorinated aromatic rings are structurally less intrusive and the exceptional sensitivity of ^{19}F chemical shifts renders them highly suitable as allosteric reporters. In the case of the Arc-NL/H11 complex, the ^{19}F chemical shift of F_5Phe in position 70 of H11 reports the ligand interaction even though all fluorine atoms are more than 10 Å from the nearest atom of Arc-NL. The simultaneous observation of at least three resonances in the ^{19}F NMR spectrum helps to detect subtle allosteric effects. Importantly, the binding affinity of the Arc-NL/H11 complex was unperturbed by the incorporation of F_5Phe residues.

CONCLUSIONS

We demonstrate that site-specific incorporation of F_5Phe enables quantitative measurement of aromatic ring-flip kinetics in proteins by shifting them into the slow-exchange regime accessible by ^{19}F NMR. This approach provides a direct probe of local protein malleability, revealing highly localized conformational fluctuations and enabling detection of minor conformational species that may be associated with cryptic binding pockets.

F_5Phe residues can be introduced with minimal structural perturbation and yield ^{19}F NMR spectra of exceptional sensitivity and resolution without isotope labeling, making the method applicable to proteins of substantial size. Changes in ring-flip rates and chemical shifts further provide a sensitive readout of allosteric effects arising from ligand binding and protein−protein interactions.

Together, these results establish fluorinated aromatic amino acids as a general strategy for engineering dynamic observables in proteins by modifying their energy landscapes. This approach should be broadly applicable for probing local conformational dynamics, mapping allosteric communication, and identifying functionally relevant conformational states in complex biomolecular systems. Site-specific incorporation of F_5Phe is inexpensive. To encourage uptake of this technology, the requisite plasmid for the aminoacyl-tRNA synthetase has been submitted to the Addgene plasmid repository (Watertown, MA, USA; plasmid no. 259751).

ASSOCIATED CONTENT

Supporting Information

The Supporting Information is available free of charge at https://pubs.acs.org/doi/10.1021/jacs.6c10121.

Experimental procedures describing materials; molecular cloning; in vivo performance of published G1-, *Ma*- and *Mb*-PylRS enzymes with F_5Phe; protein expression and purification; protein mass spectrometry; NMR spectroscopy; protein thermal stability; affinity measurements by BLI; DFT calculations of the energies of ring rotation; protein crystallization and structure determination; maximal van der Waals violations during ring rotation of F_5Phe and Phe residues; in vivo performance of G1-, *Mb*- and *Mm*-PylRS enzymes with F_5Phe; mass spectra; thermal denaturation curves; electron density of F_5Phe residues in protein crystal structures; ^{1}H-^{19}F correlation spectra 4F-Phe replacing F4, F27, or F98 in PpiB; BLI data; [^{19}F,^{19}F]-NOESY spectra; ^{19}F NMR of the dengue virus NS2B−NS3 protease; models of steric clashes during ring rotation; nucleotide and amino acid sequences; protein expression yields; crystallographic data statistics; parameters of [^{19}F,^{19}F]-NOESY spectra; BLI affinity and kinetic data for Arc-NL-F_5Phe mutants (PDF)

AUTHOR INFORMATION

Corresponding Author

Gottfried Otting − *Centre of Excellence for Innovations in Peptide and Protein Science, Research School of Chemistry, The Australian National University, Canberra, Australian Capital Territory 2601, Australia;* orcid.org/0000-0002-0563-0146; Email: gottfried.otting@anu.edu.au

Authors

Nathan Paul − *Research School of Chemistry, The Australian National University, Canberra, Australian Capital Territory 2601, Australia;* orcid.org/0009-0009-6370-3196

Adarshi P. Welegedara − *Centre of Excellence for Innovations in Peptide and Protein Science, Research School of Chemistry,*

The Australian National University, Canberra, Australian Capital Territory 2601, Australia

Rebecca L. Frkic − *Centre of Excellence for Innovations in Peptide and Protein Science, Research School of Chemistry, The Australian National University, Canberra, Australian Capital Territory 2601, Australia;* orcid.org/0000-0003-0071-9018

Luca Macri − *Research School of Chemistry, The Australian National University, Canberra, Australian Capital Territory 2601, Australia*

Toby R. C. Thompson − *Department of Chemistry, The University of Manchester, Manchester M13 9PL, U.K.;* orcid.org/0009-0004-1746-4685

James L. Baber − *Laboratory of Chemical Physics, NIDDK, NIH, Bethesda, Maryland 20892-0520, United States*

Edan Habel − *Research School of Chemistry, The Australian National University, Canberra, Australian Capital Territory 2601, Australia;* orcid.org/0009-0007-9215-8225

Elwy H. Abdelkader − *Centre of Excellence for Innovations in Peptide and Protein Science, Research School of Chemistry, The Australian National University, Canberra, Australian Capital Territory 2601, Australia;* orcid.org/0000-0002-5388-3949

Haocheng Qianzhu − *Research School of Chemistry, The Australian National University, Canberra, Australian Capital Territory 2601, Australia;* orcid.org/0000-0002-7546-4411

Nicholas F. Chilton − *Research School of Chemistry, The Australian National University, Canberra, Australian Capital Territory 2601, Australia; Department of Chemistry, The University of Manchester, Manchester M13 9PL, U.K.;* orcid.org/0000-0002-8604-0171

Colin J. Jackson − *Centre of Excellence for Innovations in Peptide and Protein Science, Research School of Chemistry, The Australian National University, Canberra, Australian Capital Territory 2601, Australia;* orcid.org/0000-0001-6150-3822

Ad Bax − *Laboratory of Chemical Physics, NIDDK, NIH, Bethesda, Maryland 20892-0520, United States;* orcid.org/0000-0002-9809-5700

Thomas Huber − *Research School of Chemistry, The Australian National University, Canberra, Australian Capital Territory 2601, Australia;* orcid.org/0000-0002-3680-8699

Complete contact information is available at: https://pubs.acs.org/10.1021/jacs.6c10121

Notes

The authors declare no competing financial interest.

■ ACKNOWLEDGMENTS

N.P. thanks the CSIRO Advanced Engineering Biology Future Science Platform and Medical Advances without Animals trust for scholarship support. We thank Prof. Martin Scanlon and Dr. Brooke Kwai for access to the 500 MHz NMR spectrometer with cryoprobe at Monash University, the Mark Wainright Analytical Centre at the University of New South Wales for access to a 600 MHz NMR spectrometer with cryoprobe, the ANU Nanobody Facility and Dr. Megan Outram for assistance with BLI experiments, and the Computational Shared Facility at The University of Manchester for computational resources. We thank the Leverhulme Trust for funding (Philip Leverhulme Prize to N.F.C. and PhD scholarship to T.R.C.T.). This research was undertaken in part using the MX3 beamline at the Australian Synchrotron, part of ANSTO. Financial support by the Australian Research Council, including the Centre of Excellence for Innovations in Peptide and Protein Science (CE200100012) and Discovery Projects (DP230100079 and DP260100191) is gratefully acknowledged. Part of this research was supported by the Intramural Research Program of the National Institute of Diabetes and Digestive and Kidney Diseases (NIDDK) within the National Institutes of Health (NIH). The contributions of the NIH authors are considered Works of the United States Government. The findings and conclusions presented in this paper are those of the authors and do not necessarily reflect the views of the NIH or the U.S. Department of Health and Human Services.

■ REFERENCES

(1) Bogan, A. A.; Thorn, K. S. Anatomy of hot spots in protein interfaces. *J. Mol. Biol.* **1998**, *280*, 1−9.

(2) Kasinath, V.; Fu, Y.; Sharp, K. A.; Wand, A. J. A sharp thermal transition of fast aromatic-ring dynamics in ubiquitin. *Angew. Chem., Int. Ed.* **2015**, *54*, 102−107.

(3) Wagner, G. Activation volumes for the rotational motion of interior aromatic rings in globular proteins determined by high resolution ^{1}H NMR at variable pressure. *FEBS Lett.* **1980**, *112*, 280−284.

(4) Wüthrich, K.; Wagner, G. NMR investigations of the dynamics of the aromatic amino acid residues in the basic pancreatic trypsin inhibitor. *FEBS Lett.* **1975**, *50*, 265−268.

(5) Campbell, I. D.; Dobson, C. M.; Moore, G. R.; Perkins, S. J.; Williams, R. J. Temperature dependent molecular motion of a tyrosine residue of ferrocytochrome C. *FEBS Lett.* **1976**, *70*, 96−100.

(6) Nall, B. T.; Zuniga, E. H. Rates and energetics of tyrosine ring flips in yeast iso-2-cytochrome-C. *Biochemistry* **1990**, *29*, 7576−7584.

(7) Hattori, M.; Li, H.; Yamada, H.; Akasaka, K.; Hengstenberg, W.; Gronwald, W.; Kalbitzer, H. R. Infrequent cavity-forming fluctuations in HPr from *Staphylococcus carnosus* revealed by pressure- and temperature-dependent tyrosine ring flips. *Protein Sci.* **2004**, *13*, 3104−3114.

(8) Krishna Rao, D.; Bhuyan, A. K. Complexity of aromatic ring-flip motions in proteins: Y97 ring dynamics in cytochrome c observed by cross-relaxation suppressed exchange NMR spectroscopy. *J. Biomol. NMR* **2007**, *39*, 187−196.

(9) Baturin, S. J.; Okon, M.; McIntosh, L. P. Structure, dynamics, and ionization equilibria of the tyrosine residues in *Bacillus circulans* xylanase. *J. Biomol. NMR* **2011**, *51*, 379−394.

(10) Yang, C.-J.; Takeda, M.; Terauchi, T.; Jee, J.; Kainosho, M. Differential large-amplitude breathing motions in the interface of FKBP12−drug complexes. *Biochemistry* **2015**, *54*, 6983−6995.

(11) Gauto, D. F.; Macek, P.; Barducci, A.; Fraga, H.; Hessel, A.; Terauchi, T.; Gajan, D.; Miyanoiri, Y.; Boisbouvier, J.; Lichtenecker, R.; Kainosho, M.; Schanda, P. Aromatic ring dynamics, thermal activation, and transient conformations of a 468 kDa enzyme by specific ^{1}H−^{13}C labeling and fast magic-angle spinning NMR. *J. Am. Chem. Soc.* **2019**, *141*, 11183−11195.

(12) Dreydoppel, M.; Raum, H. N.; Weininger, U. Slow ring flips in aromatic cluster of GB1 studied by aromatic ^{13}C relaxation dispersion methods. *J. Biomol. NMR* **2020**, *74*, 183−191.

(13) Akke, M.; Weininger, U. NMR studies of aromatic ring flips to probe conformational fluctuations in proteins. *J. Phys. Chem. B* **2023**, *127*, 591−599.

(14) Weininger, U.; Respondek, M.; Löw, C.; Akke, M. Slow aromatic ring flips detected despite near-degenerate NMR frequencies of the exchanging nuclei. *J. Phys. Chem. B* **2013**, *117*, 9241−9247.

(15) Weininger, U.; Modig, K.; Geitner, A.-J.; Schmidpeter, P. A. M.; Koch, J. R.; Akke, M. Dynamics of aromatic side chains in the active site of FKBP12. *Biochemistry* **2017**, *56*, 334−343.
(16) Dreydoppel, M.; Akke, M.; Weininger, U. Characterizing fast conformational exchange of aromatic rings using residual dipolar couplings: distinguishing jumplike flips from other exchange mechanisms. *J. Phys. Chem. B* **2022**, *126*, 7950−7956.
(17) Skalicky, J. J.; Mills, J. L.; Sharma, S.; Szyperski, T. Aromatic ring-flipping in supercooled water: implications for NMR-based structural biology of proteins. *J. Am. Chem. Soc.* **2001**, *123*, 388−397.
(18) Becker, L. M.; Fu, H.; Tatman, B. P.; Dreydoppel, M.; Kapitonova, A.; Balazs, D. M.; Weininger, U.; Engilberge, S.; Chipot, C.; Schanda, P. Aromatic ring flips reveal reshaping of protein dynamics in crystals and complexes. *Nat. Chem.* **2026**, *18*, 1221−1230.
(19) Lu, M.; Zhu, W.; Xu, G.; Chen, J.; Wu, Q.; Liu, X.; Yang, M.; Jiang, L.; Yang, M.; Liu, M.; Li, C. Characterizing tyrosine ring flips in proteins by ^{19}F NMR. *bioRxiv* **2024**, 2024.12.29.630691.
(20) Dunitz, J. D. Organic fluorine: odd man out. *ChemBioChem* **2004**, *5*, 614−621.
(21) Minnihan, E. C.; Young, D. D.; Schultz, P. G.; Stubbe, J. Incorporation of fluorotyrosines into ribonucleotide reductase using an evolved, polyspecific aminoacyl-tRNA synthetase. *J. Am. Chem. Soc.* **2011**, *133*, 15942−15945.
(22) Young, D. D.; Young, T. S.; Jahnz, M.; Ahmad, I.; Spraggon, G.; Schultz, P. G. An evolved aminoacyl-tRNA synthetase with atypical polysubstrate specificity. *Biochemistry* **2011**, *50*, 1894−1900.
(23) Wang, Y.-S.; Fang, X.; Chen, H.-Y.; Wu, B.; Wang, Z. U.; Hilty, C.; Liu, W. R. Genetic incorporation of twelve *meta*-substituted phenylalanine derivatives using a single pyrrolysyl-tRNA synthetase mutant. *ACS Chem. Biol.* **2013**, *8*, 405−415.
(24) Lee, Y.-J.; Schmidt, M. J.; Tharp, J. M.; Weber, A.; Koenig, A. L.; Zheng, H.; Gao, J.; Waters, M. L.; Summerer, D.; Liu, W. R. Genetically encoded fluorophenylalanines enable insights into the recognition of lysine trimethylation by an epigenetic reader. *Chem. Commun.* **2016**, *52*, 12606−12609.
(25) Qianzhu, H.; Abdelkader, E. H.; Herath, I. D.; Otting, G.; Huber, T. Site-specific incorporation of 7-fluoro-L-tryptophan into proteins by genetic encoding to monitor ligand binding by ^{19}F NMR spectroscopy. *ACS Sens.* **2022**, *7*, 44−49.
(26) Galles, G. D.; Infield, D. T.; Clark, C. J.; Hemshorn, M. L.; Manikandan, S.; Fazan, F.; Rasouli, A.; Tajkhorshid, E.; Galpin, J. D.; Cooley, R. B.; Mehl, R. A.; Ahern, C. A. Tuning phenylalanine fluorination to assess aromatic contributions to protein function and stability in cells. *Nat. Commun.* **2023**, *14*, 59.
(27) Zhang, Q.; Zheng, W.; Song, Z.; Zhang, Q.; Yang, L.; Wu, J.; Lin, J.; Xu, G.; Yu, H. Machine learning enables prediction of pyrrolysyl-tRNA synthetase substrate specificity. *ACS Synth. Biol.* **2023**, *12*, 2403−2417.
(28) Qianzhu, H.; Abdelkader, E. H.; Otting, G.; Huber, T. Genetic encoding of fluoro-L-tryptophans for site-specific detection of conformational heterogeneity in proteins by NMR spectroscopy. *J. Am. Chem. Soc.* **2024**, *146*, 13641−13650.
(29) Qianzhu, H.; Tan, Y. J.; Abdelkader, E. H.; Huber, T.; Otting, G. Genetic encoding of fluorinated analogues of phenylalanine for ^{19}F NMR spectroscopy: detection of conformational heterogeneity in flaviviral NS2B-NS3 proteases. *ACS Sens.* **2025**, *10*, 3152−3161.
(30) Mekkattu Tharayil, S.; Qianzhu, H.; Abdelkader, E.; Welegedara, A. P.; George, J.; Nitsche, C.; Huber, T.; Otting, G. Comparative evaluation of non-canonical amino acids as site-specific NMR probes for the complex of *E. coli* SSB with single-stranded DNA without isotope labelling. *FEBS J.* **2026**, *293*, 3601−3620.
(31) Dean, R. R.; McFarlane, W. Magnetic double resonance studies of pentafluorophenyl derivatives. *J. Chem. Soc. B* **1969**, *4*, 509−512.
(32) Mortenson, D. E.; Satyshur, K. A.; Guzei, I. A.; Forest, K. T.; Gellman, S. H. Quasiracemic crystallization as a tool to assess the accommodation of noncanonical residues in nativelike protein conformations. *J. Am. Chem. Soc.* **2012**, *134*, 2473−2476.
(33) Woll, M. G.; Hadley, E. B.; Mecozzi, S.; Gellman, S. H. Stabilizing and destabilizing effects of phenylalanine → F_5-phenylalanine mutations on the folding of a small protein. *J. Am. Chem. Soc.* **2006**, *128*, 15932−15933.
(34) Cornilescu, G.; Hadley, E. B.; Woll, M. G.; Markley, J. L.; Gellman, S. H.; Cornilescu, C. C. Solution structure of a small protein containing a fluorinated side chain in the core. *Protein Sci.* **2007**, *16*, 14−19.
(35) Dunbrack, R. L., Jr.; Karplus, M. Conformational analysis of the backbone-dependent rotamer preferences of protein sidechains. *Nat. Struct. Biol.* **1994**, *1*, 334−340.
(36) Heilshorn, S. C.; DiZio, K. A.; Welsh, E. R.; Tirrell, D. A. Endothelial cell adhesion to the fibronectin CS5 domain in artificial extracellular matrix proteins. *Biomaterials* **2003**, *24*, 4245−4252.
(37) Tan, Y. J.; Abdelkader, E. H.; Tarcoveanu, E.; Maleckis, A.; Nitsche, C.; Otting, G. (2*S*,4*S*)-5-fluoroleucine, (2*S*,4*R*)-5-fluoroleucine, and 5,5′-difluoroleucine in *E. coli* PpiB: protein production, ^{19}F NMR, and ligand sensing enhanced by the γ-gauche effect. *Biochemistry* **2024**, *63*, 1376−1387.
(38) Tan, Y. J.; Abdelkader, E. H.; Herath, I. D.; Maleckis, A.; Otting, G. Inter-residue through-space scalar ^{19}F−^{19}F couplings between CH_2F groups in a protein. *Magn. Reson.* **2025**, *6*, 131−142.
(39) Edwards, K. J.; Ollis, D. L.; Dixon, N. E. Crystal structure of cytoplasmic *Escherichia coli* peptidyl-prolyl isomerase: evidence for decreased mobility of loops upon complexation. *J. Mol. Biol.* **1997**, *271*, 258−265.
(40) Godoy Muñoz, J. M.; Neset, L.; Markússon, S.; Weber, S.; Krokengen, O. C.; Sutinen, A.; Christakou, E.; Lopez, A. J.; Bramham, C. R.; Kursula, P. Structural characterization of two nanobodies targeting the ligand-binding pocket of human Arc. *PLoS One* **2024**, *19*, No. e0300453.
(41) Frericks Schmidt, H. L.; Sperling, L. J.; Gao, Y. G.; Wylie, B. J.; Boettcher, J. M.; Wilson, S. R.; Rienstra, C. M. Crystal polymorphism of protein GB1 examined by solid-state NMR spectroscopy and X-ray diffraction. *J. Phys. Chem. B* **2007**, *111*, 14362−14369.
(42) Dreydoppel, M.; Lichtenecker, R. J.; Akke, M.; Weininger, U. ^{1}H $R_{1\rho}$ relaxation dispersion experiments in aromatic side chains. *J. Biomol. NMR* **2021**, *75*, 383−392.
(43) Van Duyne, G. D.; Standaert, R. F.; Schreiber, S. L.; Clardy, J. Atomic structure of the rapamycin human immunophilin FKBP-12 complex. *J. Am. Chem. Soc.* **1991**, *113*, 7433−7434.
(44) Quiocho, F. A.; Spurlino, J. C.; Rodseth, L. E. Extensive features of tight oligosaccharide binding revealed in high-resolution structures of the maltodextrin transport/chemosensory receptor. *Structure* **1997**, *5*, 997−1015.
(45) Kainosho, M.; Torizawa, T.; Iwashita, Y.; Terauchi, T.; Mei Ono, A.; Güntert, P. Optimal isotope labelling for NMR protein structure determinations. *Nature* **2006**, *440*, 52−57.
(46) Sharff, A. J.; Rodseth, L. E.; Spurlino, J. C.; Quiocho, F. A. Crystallographic evidence of a large ligand-induced hinge-twist motion between the two domains of the maltodextrin binding protein involved in active transport and chemotaxis. *Biochemistry* **1992**, *31*, 10657−10663.
(47) Lilkova, E. *The PyMOL Molecular Graphics System, Version 2.0*; Schrödinger, LLC, 2015.
(48) Erbel, P.; Schiering, N.; D'Arcy, A.; Renatus, M.; Kroemer, M.; Lim, S. P.; Yin, Z.; Keller, T. H.; Vasudevan, S. G.; Hommel, U. Structural basis for the activation of flaviviral NS3 proteases from dengue and West Nile virus. *Nat. Struct. Mol. Biol.* **2006**, *13*, 372−373.
(49) Aleshin, A. E.; Shiryaev, S. A.; Strongin, A. Y.; Liddington, R. C. Structural evidence for regulation and specificity of flaviviral proteases and evolution of the *Flaviviridae* fold. *Protein Sci.* **2007**, *16*, 795−806.
(50) de la Cruz, L.; Nguyen, T. H. D.; Ozawa, K.; Shin, J.; Graham, B.; Huber, T.; Otting, G. Binding of low-molecular weight inhibitors promotes large conformational changes in the dengue virus NS2B-NS3 protease: fold analysis by pseudocontact shifts. *J. Am. Chem. Soc.* **2011**, *133*, 19205−19215.
(51) Ramanujam, V.; Alderson, T. R.; Pritišanac, I.; Ying, J.; Bax, A. Protein structural changes characterized by high-pressure, pulsed field

gradient diffusion NMR spectroscopy. *J. Magn. Reson.* **2020**, *312*, 106701.
(52) Wagner, G.; Brühwiler, D.; Wüthrich, K. Reinvestigation of the aromatic side-chains in the basic pancreatic trypsin inhibitor by heteronuclear two-dimensional nuclear magnetic resonance. *J. Mol. Biol.* **1987**, *196*, 227−231.
(53) Pace, C. J.; Gao, J. Exploring and exploiting polar−π interactions with fluorinated aromatic amino acids. *Acc. Chem. Res.* **2013**, *46*, 907−915.
(54) Hoffmann, W.; Langenhan, J.; Huhmann, S.; Moschner, J.; Chang, R.; Accorsi, M.; Seo, J.; Rademann, J.; Meijer, G.; Koksch, B.; Bowers, M. T.; von Helden, G.; Pagel, K. An intrinsic hydrophobicity scale for amino acids and its application to fluorinated compounds. *Angew. Chem., Int. Ed.* **2019**, *58*, 8216−8220.
(55) Chiu, H.-P.; Suzuki, Y.; Gullickson, D.; Ahmad, R.; Kokona, B.; Fairman, R.; Cheng, R. P. Helix propensity of highly fluorinated amino acids. *J. Am. Chem. Soc.* **2006**, *128*, 15556−15557.
(56) Chiu, H.-P.; Kokona, B.; Fairman, R.; Cheng, R. P. Effect of highly fluorinated amino acids on protein stability at a solvent-exposed position on an internal strand of protein G B1 domain. *J. Am. Chem. Soc.* **2009**, *131*, 13192−13193.
(57) Zheng, H.; Gao, J. Highly specific heterodimerization mediated by quadrupole interactions. *Angew. Chem., Int. Ed.* **2010**, *49*, 8635−8639.
(58) Kitevski-LeBlanc, J. L.; Evanics, F.; Prosser, R. S. Optimizing ^{19}F NMR protein spectroscopy by fractional biosynthetic labeling. *J. Biomol. NMR* **2010**, *48*, 113−121.
(59) Welte, H.; Zhou, T.; Mihajlenko, X.; Mayans, O.; Kovermann, M. What does fluorine do to a protein? Thermodynamic, and highly-resolved structural insights into fluorine-labelled variants of the cold shock protein. *Sci. Rep.* **2020**, *10*, 2640.
(60) Streit, J. O.; Bukvin, I. V.; Chan, S. H. S.; Bashir, S.; Woodburn, L. F.; Włodarski, T.; Figueiredo, A. M.; Jurkeviciute, G.; Sidhu, H. K.; Hornby, C. R.; Waudby, C. A.; Cabrita, L. D.; Cassaignau, A. M. E.; Christodoulou, J. The ribosome lowers the entropic penalty of protein folding. *Nature* **2024**, *633*, 232−239.
(61) Kulkarni, M.; Söderhjelm, P. Free-energy landscape and rate estimation of the aromatic ring flips in basic pancreatic trypsin inhibitors using metadynamics. *J. Chem. Theory Comput.* **2023**, *19*, 6605−6618.
(62) Li, H.; Yamada, H.; Akasaka, K. Effect of pressure on the tertiary structure and dynamics of folded basic pancreatic trypsin inhibitor. *Biophys. J.* **1999**, *77*, 2801−2812.
(63) Kramers, H. A. Brownian motion in a field of force and the diffusion model of chemical reactions. *Physica* **1940**, *7*, 284−304.
(64) Beece, D.; Eisenstein, L.; Frauenfelder, H.; Good, D.; Marden, M. C.; Reinisch, L.; Reynolds, A. H.; Sorensen, L. B.; Yue, K. T. Solvent viscosity and protein dynamics. *Biochemistry* **1980**, *19*, 5147−5157.
(65) Dreydoppel, M.; Dorn, B.; Modig, K.; Akke, M.; Weininger, U. Transition-state compressibility and activation volume of transient protein conformational fluctuations. *JACS Au* **2021**, *1*, 833−842.
(66) Qianzhu, H.; Abdelkader, E. H.; Welegedara, A. P.; Habel, E.; Paul, N.; Frkic, R. L.; Jackson, C. J.; Huber, T.; Otting, G. Rendering proteins fluorescent inconspicuously: genetically encoded 4-cyano-tryptophan conserves their structure and enables the detection of ligand binding sites. *Angew. Chem., Int. Ed.* **2024**, *64*, No. e202421000.

https://doi.org/10.1021/jacs.6c10121
J. Am. Chem. Soc. 2026, 148, 32644−32655